

Local MFS Matrix Decomposition Algorithms for Elliptic BVPs in Annuli

C.S. Chen¹, Andreas Karageorghis² and Min Lei^{3,*}

¹ School of Mathematics and Natural Sciences, University of Southern Mississippi, Hattiesburg, MS 39406, USA

² Department of Mathematics and Statistics, University of Cyprus, P.O. Box 20537, Nicosia 1678, Cyprus

³ College of Mathematics, Taiyuan University of Technology, Taiyuan 030024, P.R. China

Received 17 April 2023; Accepted (in revised version) 11 September 2023

Abstract. We apply the local method of fundamental solutions (LMFS) to boundary value problems (BVPs) for the Laplace and homogeneous biharmonic equations in annuli. By appropriately choosing the collocation points, the LMFS discretization yields sparse block circulant system matrices. As a result, matrix decomposition algorithms (MDAs) and fast Fourier transforms (FFTs) can be used for the solution of the systems resulting in considerable savings in both computational time and storage requirements. The accuracy of the method and its ability to solve large scale problems are demonstrated by applying it to several numerical experiments.

AMS subject classifications: Primary 65N35; Secondary 65N22

Key words: Local method of fundamental solutions, Poisson equation, biharmonic equation, matrix decomposition algorithms, fast Fourier transforms.

1. Introduction

The method of fundamental solutions (MFS) was introduced as a numerical method several decades ago [9, 28] and is by now an established method for accurately and effectively solving certain elliptic boundary value problems (BVPs) [7, 10, 14]. It is a boundary meshless method applicable to BVPs in which the fundamental solutions of the operators of the governing partial differential equations (PDEs) are known. The main attraction of the MFS is its simplicity since only the location of the boundary nodes (and corresponding sources) is required and neither interior discretization nor boundary integration are needed. As such, the MFS can be used to solve many complicated

*Corresponding author. *Email addresses:* cs.chen@usm.edu (C.S. Chen), andreask@ucy.ac.cy (A. Karageorghis), leimin@tyut.edu.cn (M. Lei)

problems in science and engineering. However, identifying the source location (outside the domain) to yield optimal accuracy remains a challenge. In particular, when the domain is multi-connected containing several small cavities, placing the source points appropriately is a far from trivial task. It should be noted that the geometric shape of the domain and the boundary conditions (BCs) can affect the optimal source location. In theory, there are infinite ways of selecting the positions of the source points and many studies have attempted to resolve this issue. Moreover, since the traditional MFS is a global method and not a local method, the matrix resulting from such a discretization is full and poorly-conditioned. For large-scale problems requiring a large number of collocation points, implementationally demanding techniques such as domain decomposition or the fast multipole method need to be employed, which defeats the purpose of using the MFS in the first place since, as stated earlier, its major attraction is its simplicity. The above issues are, to a large extent, overcome in a recently developed local version of the MFS which yields sparse matrices. More specifically, the local method of fundamental solutions (LMFS) was introduced in the key paper [11] and has since been applied for the solution of a large variety of problems [4–6, 12, 15–19, 23–26, 29–31, 33–36].

The LMFS combines the traditional MFS with the ideas developed in other local meshless methods. As a result, in the implementation of the LMFS, both boundary and interior nodes are required and, technically speaking, it may no longer be classified as a boundary method. Hence, we can consider the LMFS as a hybrid method combining features from both boundary and domain discretization methods. Fortunately however, the LMFS inherits the simplicity of the MFS.

The matrix resulting from the LMFS discretization is sparse which means that the corresponding linear systems can be efficiently solved. However, when the number of boundary and interior points becomes extremely large, the memory storage space and computational CPU time required become a problem.

In the current work we shall apply matrix decomposition algorithms (MDAs) [1] for the solution of Laplacian and biharmonic BVPs in annular domains. In MDAs, global systems (which could be sparse) are decomposed into many small systems, the solution of which results in substantial savings in both computational time and storage. Such algorithms have been employed extensively in MFS formulations, see e.g. [21]. MDAs have also been applied to radial basis function (RBF) collocation methods [27] and, in particular, to the local RBF method [2] which shares several features with the LMFS. In this paper, we apply MDAs to the LMFS to form an even more powerful meshless method which, as will be demonstrated, can readily handle problems with one million collocation nodes without the need of a high performance computer.

The types of BVPs examined in this study are presented in Section 2. In Section 3 we provide a detailed description of the LMFS for the solution of BVPs governed by the Laplace equation. The LMFS for biharmonic BVPs is presented in Section 4 while an alternative formulation for such problems is given in Section 5. In Section 7 we analyze the results obtained when the proposed method is applied to various test problems. Finally, we conclude with some comments and ideas about future work in Section 8.

2. The problems

2.1. Laplacian problems

We study the BVP, which consists of the Laplace equation

$$\Delta u = 0 \quad \text{in } \Omega, \quad (2.1a)$$

and the boundary conditions

$$u = g_1^D \quad \text{on } \partial\Omega_1, \quad (2.1b)$$

and

$$u = g_2^D \quad \text{on } \partial\Omega_2, \quad (2.1c)$$

or

$$\frac{\partial u}{\partial \mathbf{n}} = g_2^N \quad \text{on } \partial\Omega_2, \quad (2.1d)$$

in the annulus

$$\Omega = \{ \mathbf{x} \in \mathbb{R}^2 : \varrho_1 < |\mathbf{x}| < \varrho_2 \}. \quad (2.2)$$

In (2.1) g_1^D, g_2^D and g_2^N are given functions and the boundary $\partial\Omega = \partial\Omega_1 \cup \partial\Omega_2$, $\partial\Omega_1 \cap \partial\Omega_2 = \emptyset$, where

$$\partial\Omega_1 = \{ \mathbf{x} \in \mathbb{R}^2 : |\mathbf{x}| = \varrho_1 \}, \quad \partial\Omega_2 = \{ \mathbf{x} \in \mathbb{R}^2 : |\mathbf{x}| = \varrho_2 \}.$$

In (2.1d), $\partial/\partial \mathbf{n}$ denotes the derivative along the outward unit normal vector $\mathbf{n} = (n_x, n_y)$ to $\partial\Omega$. Clearly, (2.1a), (2.1b) and (2.1c) compose a Dirichlet BVP, whereas (2.1a), (2.1d), and (2.1c) a mixed Dirichlet-Neumann BVP.

2.2. Biharmonic problems

We also examine the homogeneous biharmonic equation

$$\Delta^2 u = 0 \quad \text{in } \Omega, \quad (2.3a)$$

subject to either the BCs

$$u = g_k^D \quad \text{and} \quad \frac{\partial u}{\partial \mathbf{n}} = g_k^N \quad \text{on } \partial\Omega_k, \quad k = 1, 2, \quad (2.3b)$$

or the BCs

$$u = g_k^D \quad \text{and} \quad \Delta u = g_k^L \quad \text{on } \partial\Omega_k, \quad k = 1, 2, \quad (2.3c)$$

where g_k^D, g_k^N and $g_k^L, k = 1, 2$, are given functions. BVP (2.3a)-(2.3b) is the first biharmonic problem and, the BVP consisting of (2.3a) and (2.3c), the second biharmonic problem. In elasticity, the former problem corresponds to a clamped plate whereas the latter problem corresponding to a simply-supported plate. The domain Ω in the above BVPs in depicted in Fig. 1(a).

3. Laplacian problems

3.1. Collocation point distribution

The \mathcal{K} collocation point (nodes) set $\mathcal{X} = \{\mathbf{x}_i\}_{i=1}^{\mathcal{K}}$ in $\overline{\Omega}$ is constructed as follows. We define the M angles

$$\vartheta_m = \frac{2\pi(m-1)}{M}, \quad m = 1, \dots, M, \quad (3.1)$$

and the N radii

$$r_n = \varrho_1 + (\varrho_2 - \varrho_1) \frac{n-1}{N-1}, \quad n = 1, \dots, N. \quad (3.2)$$

We then define the collocation points $\{(x_{mn}, y_{mn})\}_{m=1, n=1}^{M, N}$ by

$$x_{mn} = r_n \cos \theta_{mn}, \quad y_{mn} = r_n \sin \theta_{mn}, \quad m = 1, \dots, M, \quad n = 1, \dots, N, \quad (3.3)$$

where

$$\theta_{mn} = \vartheta_m + \frac{2\pi s_n}{M}.$$

In (3.3) the parameters $\{s_n\}_{n=1}^N \in [-1/2, 1/2]$ result in rotations of the nodes and produce more uniform collocation-point distributions, see e.g. [2]. A representative collocation point distribution is shown in Fig. 1(b).

We take the \mathcal{K}_{int} interior points $\mathcal{X}_{\text{int}} = \{\mathbf{x}_i\}_{i=1}^{\mathcal{K}_{\text{int}}}$ to be

$$\mathbf{x}_{(n-2)M+m} = (x_{mn}, y_{mn}), \quad m = 1, \dots, M, \quad n = 2, \dots, N-1, \quad (3.4)$$

and the \mathcal{K}_{bry} boundary points $\mathcal{X}_{\text{bry}} = \{\mathbf{x}_i\}_{i=\mathcal{K}_{\text{int}}+1}^{\mathcal{K}_{\text{int}}+\mathcal{K}_{\text{bry}}}$ as

$$\mathbf{x}_{(N-2)M+m} = (x_{m1}, y_{m1}), \quad \mathbf{x}_{(N-1)M+m} = (x_{mN}, y_{mN}), \quad m = 1, \dots, M, \quad (3.5)$$

where, clearly, $\mathcal{X} = \mathcal{X}_{\text{int}} \cup \mathcal{X}_{\text{bry}}$, $\mathcal{X}_{\text{int}} \cap \mathcal{X}_{\text{bry}} = \emptyset$, $\mathcal{K}_{\text{int}} = (N-2)M$, $\mathcal{K}_{\text{bry}} = 2M$ and $\mathcal{K} = MN$. The points $\{\mathbf{x}_i\}_{i=\mathcal{K}_{\text{int}}+1}^{\mathcal{K}_{\text{int}}+\mathcal{K}_{\text{bry}}}$ are the boundary points on $\partial\Omega_1$ and the points

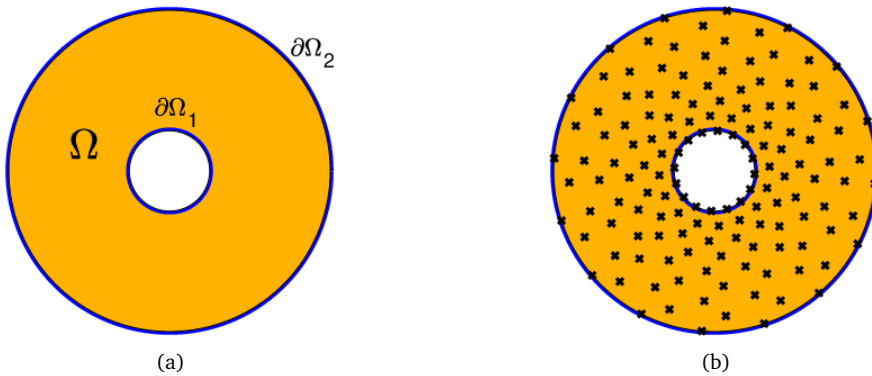


Figure 1: (a) Geometry of problems under consideration. (b) Typical distribution of collocation points for Laplacian BVPs.

$\{\mathbf{x}_i\}_{i=\mathcal{K}_{\text{int}}+\mathcal{K}_{\text{bry}_1}+1}^{\mathcal{K}}$ are the boundary points on $\partial\Omega_2$. Obviously, $\mathcal{K}_{\text{bry}} = \mathcal{K}_{\text{bry}_1} + \mathcal{K}_{\text{bry}_2}$ and $\mathcal{K} = \mathcal{K}_{\text{int}} + \mathcal{K}_{\text{bry}_1} + \mathcal{K}_{\text{bry}_2}$. For any node $\mathbf{x}_i \in \mathcal{X}$, we select the nearest κ nodes in \mathcal{X} (excluding \mathbf{x}_i). These form a set $\mathcal{X}_i = \{\mathbf{x}_\ell^i\}_{\ell=1}^{\kappa}$ and are indexed locally as $\mathbf{x}_\ell^i = \mathbf{x}_{\ell(i)}$. Moreover, they lie in the local influence domain of the node which we shall denote by Ω_i . These overlapping sets of points $(\mathcal{X}_i)_{i=1}^{\mathcal{K}}$ are such that $\{\mathbf{x}_i\}_{i=1}^{\mathcal{K}} = \bigcup_{i=1}^{\mathcal{K}} \mathcal{X}_i = \mathcal{X}$. Clearly, a crucial issue in the application of the LMFS is the selection of the κ nearest nodes to \mathbf{x}_i in \mathcal{X} for each Ω_i . This can be achieved using the KD-tree algorithm [13] which partitions an $n \times K$ data set by recursively splitting n points in a K -dimensional space into a binary tree. The building and storing of the KD binary tree is obtained via the MATLAB[®] command `KDTreeSearch`. Once the KD-tree has been established, one can search the stored tree to find all neighbouring points to the query data by performing a nearest neighbour search using the MATLAB[®] command `knnsearch`.

3.2. The LMFS

For any node \mathbf{x}_i in \mathcal{X} we first select the κ nearest nodes $\mathcal{X}_i = \{\mathbf{x}_\ell^i\}_{\ell=1}^{\kappa}$ in \mathcal{X} . We then choose κ sources on a circle around Ω_i which we shall denote by $\{\boldsymbol{\xi}_\ell^i\}_{\ell=1}^{\kappa}$. These are defined by

$$\boldsymbol{\xi}_\ell^{(n-1)M+m} = \mathbf{x}_{(n-1)M+m} + R_{mn} \left(\cos \left(\frac{2(\ell-1)\pi}{\kappa} + \theta_{mn} \right), \sin \left(\frac{2(\ell-1)\pi}{\kappa} + \theta_{mn} \right) \right), \quad (3.6)$$

$\ell = 1, \dots, \kappa$, $m = 1, \dots, M$, $n = 1, \dots, N$, where R_{mn} is an appropriately chosen radius. Note that often we choose the same radius R for each Ω_i , that is $R_{mn} = R$, $m = 1, \dots, M$, $n = 1, \dots, N$. A typical distribution of nodes in Ω_i and the corresponding sources is depicted in Fig. 2(a). It is important to stress that the source number could be chosen to be $\kappa_1 < \kappa$ without affecting the proposed algorithm.

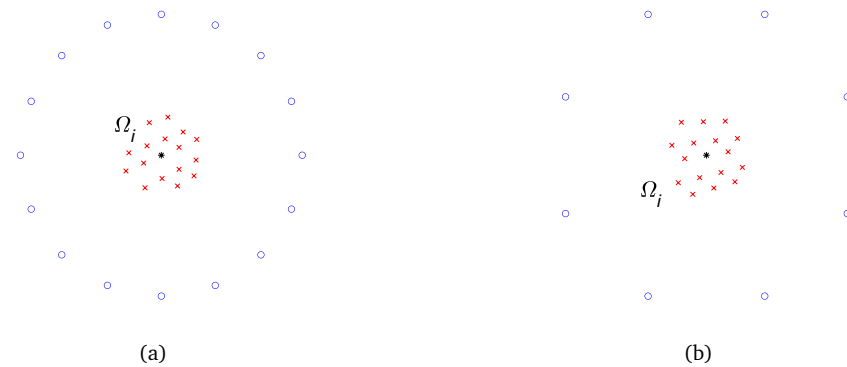


Figure 2: Simplified typical distribution of collocation points (\times) and corresponding sources (\circ) for domain Ω_i around point \mathbf{x}_i (*): (a) Laplacian. (b) Biharmonic.

If \mathbf{x}_i is an interior node – i.e. $\mathbf{x}_i \in \mathcal{X}_{\text{int}}$, motivated by the fact that in the domain Ω_i the solution u satisfies the Laplace equation, we consider the local MFS approximation

$$u^{(i)}(\mathbf{x}) = \sum_{\ell=1}^{\kappa} \alpha_{\ell}^i G_L(\mathbf{x}, \boldsymbol{\xi}_{\ell}^i), \quad \mathbf{x} \in \bar{\Omega}_i, \quad (3.7)$$

where G_L is a fundamental solution of the Laplace operator, defined by

$$G_L(\mathbf{x}, \boldsymbol{\xi}) = \frac{1}{2\pi} \ln |\mathbf{x} - \boldsymbol{\xi}|, \quad (3.8)$$

and $\{\alpha_{\ell}^i\}_{\ell=1}^{\kappa}$ are unknown coefficients. We next collocate (3.7) at each of the points \mathbf{x}_{ℓ}^i , $\ell = 1, \dots, \kappa$, which yields

$$\begin{aligned} \begin{bmatrix} u^{(i)}(\mathbf{x}_1^i) \\ u^{(i)}(\mathbf{x}_2^i) \\ \vdots \\ u^{(i)}(\mathbf{x}_{\kappa}^i) \end{bmatrix} &= \begin{bmatrix} u_1^{(i)} \\ u_2^{(i)} \\ \vdots \\ u_{\kappa}^{(i)} \end{bmatrix} \\ &= \begin{bmatrix} G_L(\mathbf{x}_1^i - \boldsymbol{\xi}_1^i) & G_L(\mathbf{x}_1^i - \boldsymbol{\xi}_2^i) & \cdots & G_L(\mathbf{x}_1^i - \boldsymbol{\xi}_{\kappa}^i) \\ G_L(\mathbf{x}_2^i - \boldsymbol{\xi}_1^i) & G_L(\mathbf{x}_2^i - \boldsymbol{\xi}_2^i) & \cdots & G_L(\mathbf{x}_2^i - \boldsymbol{\xi}_{\kappa}^i) \\ \vdots & \vdots & \vdots & \vdots \\ G_L(\mathbf{x}_{\kappa}^i - \boldsymbol{\xi}_1^i) & G_L(\mathbf{x}_{\kappa}^i - \boldsymbol{\xi}_2^i) & \cdots & G_L(\mathbf{x}_{\kappa}^i - \boldsymbol{\xi}_{\kappa}^i) \end{bmatrix} \begin{bmatrix} \alpha_1^i \\ \alpha_2^i \\ \vdots \\ \alpha_{\kappa}^i \end{bmatrix} \end{aligned} \quad (3.9)$$

or with the obvious notation

$$\mathbf{u}^{(i)} = \mathbf{G}_L^{(i)} \boldsymbol{\alpha}^i. \quad (3.10)$$

Assuming that the $\kappa \times \kappa$ matrix $\mathbf{G}_L^{(i)}$ is invertible, we have

$$\boldsymbol{\alpha}^i = \mathbf{G}_L^{(i)-1} \mathbf{u}^{(i)}. \quad (3.11)$$

As mentioned in [11], since each local coefficient matrix $\mathbf{G}_L^{(i)}$ is ill-conditioned, it is advisable to use the MATLAB[®] function `pinv` to evaluate its inverse in (3.11) setting the tolerance at 10^{-8} . We then apply (3.7) at $\mathbf{x} = \mathbf{x}_i$, and from (3.11), get

$$\begin{aligned} u^{(i)}(\mathbf{x}_i) &= \sum_{\ell=1}^{\kappa} \alpha_{\ell}^i G_L(\mathbf{x}_i, \boldsymbol{\xi}_{\ell}^i) \\ &= [G_L(\mathbf{x}_i, \boldsymbol{\xi}_1^i) \ G_L(\mathbf{x}_i, \boldsymbol{\xi}_2^i) \ \cdots \ G_L(\mathbf{x}_i, \boldsymbol{\xi}_{\kappa}^i)] \boldsymbol{\alpha}^i \\ &= [G_L(\mathbf{x}_i, \boldsymbol{\xi}_1^i) \ G_L(\mathbf{x}_i, \boldsymbol{\xi}_2^i) \ \cdots \ G_L(\mathbf{x}_i, \boldsymbol{\xi}_{\kappa}^i)] \mathbf{G}_L^{(i)-1} \mathbf{u}^{(i)} \\ &= \mathbf{w}^{(i)} \mathbf{u}^{(i)} \\ &= \sum_{\ell=1}^{\kappa} w_{\ell}^{(i)} u_{\ell}^{(i)}, \end{aligned} \quad (3.12)$$

where the row vector $\mathbf{w}^{(i)}$ is defined by

$$\mathbf{w}^{(i)} = [G_L(\mathbf{x}_i, \boldsymbol{\xi}_1^i) \ G_L(\mathbf{x}_i, \boldsymbol{\xi}_2^i) \ \cdots \ G_L(\mathbf{x}_i, \boldsymbol{\xi}_\kappa^i)] \mathbf{G}_L^{(i)-1}. \quad (3.13)$$

From (3.12) we obtain a finite difference-type equation linking the approximate values of u at all nodes in $\Omega^{(i)}$ (including \mathbf{x}_i), and by applying this to every interior node we generate the set of equations

$$u^{(i)}(\mathbf{x}_i) - \sum_{\ell=1}^{\kappa} w_\ell^{(i)} u_\ell^{(i)} = u_i - \sum_{\ell=1}^{\kappa} w_\ell^{(i)} u_\ell^{(i)} = 0, \quad i = 1, \dots, \mathcal{K}_{\text{int}}. \quad (3.14)$$

To these \mathcal{K}_{int} equations, in the case of a Dirichlet BVP, we need to add the Dirichlet BCs (2.1b) and (2.1c) for $\mathbf{x}_i \in \mathcal{X}_{\text{bry}}$

$$u(\mathbf{x}_i) = u_i = g_1^D(\mathbf{x}_i), \quad i = \mathcal{K}_{\text{int}} + 1, \dots, \mathcal{K}_{\text{int}} + \mathcal{K}_{\text{bry}_1}, \quad (3.15)$$

$$u(\mathbf{x}_i) = u_i = g_2^D(\mathbf{x}_i), \quad i = \mathcal{K}_{\text{int}} + \mathcal{K}_{\text{bry}_1} + 1, \dots, \mathcal{K}_{\text{int}} + \mathcal{K}_{\text{bry}}. \quad (3.16)$$

For a Neumann BC (2.1d) on $\partial\Omega_2$, by differentiating (3.7) we have

$$\frac{\partial u^{(i)}}{\partial \mathbf{n}}(\mathbf{x}) = \sum_{\ell=1}^{\kappa} \alpha_\ell^i \frac{\partial G_L}{\partial \mathbf{n}}(\mathbf{x}, \boldsymbol{\xi}_\ell^i), \quad (3.17)$$

which, when applied at $\mathbf{x} = \mathbf{x}_i \in \mathcal{X}_{\text{bry}}$ on $\partial\Omega_2$ in combination with (3.10) yields

$$\begin{aligned} g_2^N(\mathbf{x}_i) &= \frac{\partial u^{(i)}}{\partial \mathbf{n}}(\mathbf{x}_i) \\ &= \sum_{\ell=1}^{\kappa} \alpha_\ell^i \frac{\partial G_L}{\partial \mathbf{n}}(\mathbf{x}_i, \boldsymbol{\xi}_\ell^i) \\ &= \left[\frac{\partial G_L}{\partial \mathbf{n}}(\mathbf{x}_i, \boldsymbol{\xi}_1^i) \ \frac{\partial G_L}{\partial \mathbf{n}}(\mathbf{x}_i, \boldsymbol{\xi}_2^i) \ \cdots \ \frac{\partial G_L}{\partial \mathbf{n}}(\mathbf{x}_i, \boldsymbol{\xi}_\kappa^i) \right] \boldsymbol{\alpha}^i \\ &= \left[\frac{\partial G_L}{\partial \mathbf{n}}(\mathbf{x}_i, \boldsymbol{\xi}_1^i) \ \frac{\partial G_L}{\partial \mathbf{n}}(\mathbf{x}_i, \boldsymbol{\xi}_2^i) \ \cdots \ \frac{\partial G_L}{\partial \mathbf{n}}(\mathbf{x}_i, \boldsymbol{\xi}_\kappa^i) \right] \mathbf{G}_L^{(i)-1} \mathbf{u}^{(i)} \\ &= \mathbf{w}_n^{(i)} \mathbf{u}^{(i)} \\ &= \sum_{\ell=1}^{\kappa} w_{\ell_n}^{(i)} u_\ell^{(i)}, \end{aligned} \quad (3.18)$$

where

$$\begin{aligned} \mathbf{w}_n^{(i)} &= \left[\frac{\partial G_L}{\partial \mathbf{n}}(\mathbf{x}_i, \boldsymbol{\xi}_1^i) \ \frac{\partial G_L}{\partial \mathbf{n}}(\mathbf{x}_i, \boldsymbol{\xi}_2^i) \ \cdots \ \frac{\partial G_L}{\partial \mathbf{n}}(\mathbf{x}_i, \boldsymbol{\xi}_\kappa^i) \right] \mathbf{G}_L^{(i)-1}, \\ \frac{\partial G_L}{\partial \mathbf{n}}(\mathbf{x}_i, \boldsymbol{\xi}_\ell^i) &= n_{x_i} \frac{\partial G_L}{\partial x}(\mathbf{x}_i, \boldsymbol{\xi}_\ell^i) + n_{y_i} \frac{\partial G_L}{\partial y}(\mathbf{x}_i, \boldsymbol{\xi}_\ell^i) \end{aligned} \quad (3.19)$$

with

$$\frac{\partial G_L}{\partial x}(\mathbf{x}, \boldsymbol{\xi}) = \frac{1}{2\pi} \frac{x - \xi_x}{|\mathbf{x} - \boldsymbol{\xi}|^2}, \quad \frac{\partial G_L}{\partial y}(\mathbf{x}, \boldsymbol{\xi}) = \frac{1}{2\pi} \frac{y - \xi_y}{|\mathbf{x} - \boldsymbol{\xi}|^2}, \quad (3.20)$$

and

$$\mathbf{x} = (x, y), \quad \boldsymbol{\xi} = (\xi_x, \xi_y).$$

From (3.18) we again obtain a finite difference-type equation linking the approximate values of all nodes in $\Omega^{(i)}$ (now excluding the boundary node \mathbf{x}_i), and by applying this to every boundary node on $\partial\Omega_2$, instead of Eqs. (3.16), we get the set of equations

$$\sum_{\ell=1}^{\kappa} w_{\ell_n}^{(i)} u_{\ell}^{(i)} = g_2^N(\mathbf{x}_i), \quad i = \mathcal{K}_{\text{int}} + \mathcal{K}_{\text{bry}_1} + 1, \dots, \mathcal{K}_{\text{int}} + \mathcal{K}_{\text{bry}}. \quad (3.21)$$

The assembly of the equations corresponding to all \mathcal{K} nodes $\mathbf{x}_i \in \mathcal{X}$, namely (3.14), (3.15) and (3.16) or (3.21), results in a $\mathcal{K} \times \mathcal{K}$ system

$$A \mathbf{u}_{\mathcal{K}} = \mathbf{b}, \quad (3.22)$$

where $A \in \mathbb{R}^{\mathcal{K} \times \mathcal{K}}$ is a sparse matrix and the vector $\mathbf{b} = [b_1, \dots, b_{\mathcal{K}}]^T$ is given by

$$\begin{aligned} b_i &= 0, & i &= 1, \dots, \mathcal{K}_{\text{int}}, \\ b_i &= g_1^D(\mathbf{x}_i), & i &= \mathcal{K}_{\text{int}} + 1, \dots, \mathcal{K}_{\text{int}} + \mathcal{K}_{\text{bry}_1}, \\ b_i &= g_2^D(\mathbf{x}_i) \quad \text{or} \quad g_2^N(\mathbf{x}_i), & i &= \mathcal{K}_{\text{int}} + \mathcal{K}_{\text{bry}_1} + 1, \dots, \mathcal{K}_{\text{int}} + \mathcal{K}_{\text{bry}_1} + \mathcal{K}_{\text{bry}_2}. \end{aligned}$$

Solving system (3.22) for $\mathbf{u}_{\mathcal{K}} \in \mathbb{R}^{\mathcal{K} \times 1}$ yields the solution u approximations at the nodes in \mathcal{X} . More specifically, if $\mathbf{u}_{\mathcal{K}} = [u_{\mathcal{K}_1}, \dots, u_{\mathcal{K}_{\mathcal{K}}}]^T$, then $u_{\mathcal{K}_i}$ denotes the solution approximation at the node \mathbf{x}_i , $i = 1, \dots, \mathcal{K}$.

In the present case, with the distribution of collocation points described in Section 3.1, system (3.22) has the special structure

$$A \mathbf{u} = \begin{bmatrix} A_{1,1} & A_{1,2} & \dots & A_{1,N} \\ A_{2,1} & A_{2,2} & \dots & A_{2,N} \\ \vdots & \vdots & \ddots & \vdots \\ A_{N,1} & A_{N,2} & \dots & A_{N,N} \end{bmatrix} \begin{bmatrix} \mathbf{u}_1 \\ \mathbf{u}_2 \\ \vdots \\ \mathbf{u}_N \end{bmatrix} = \begin{bmatrix} \mathbf{b}_1 \\ \mathbf{b}_2 \\ \vdots \\ \mathbf{b}_N \end{bmatrix} = \mathbf{b}, \quad (3.23)$$

where $M \times M$ submatrices A_{n_1, n_2} , $n_1, n_2 = 1, \dots, N$, are sparse circulants [8]. In other words, A in (3.23) is a block circulant matrix consisting of sparse blocks. Consequently, the MDA described in the Appendix may be employed for the efficient solution of system (3.23). Each $M \times M$ submatrix A_{n_1, n_2} in (3.23) is circulant because the configuration of the neighbouring points $\{\mathbf{x}_{\ell}^i\}_{\ell=1}^{\kappa}$ around point \mathbf{x}_i and the corresponding sources $\{\boldsymbol{\xi}_{\ell}\}_{\ell=1}^{\kappa}$ as depicted in Fig. 2(a) will be repeated for each point \mathbf{x}_i on each concentric circle around the origin. This means that the appropriate node-source distances will be the same, leading to the same intermediate vectors/matrices in (3.13) and hence to the same coefficients $w_{\ell}^{(i)}$ in (3.12). In other words, the coefficients linking each point

\mathbf{x}_i to its κ neighbouring points are the same for each point on each different concentric circle. This yields a circulant matrix for the set of points \mathbf{x}_i lying on the same concentric circle. A similar argument holds for the imposition of the Neumann BC on the outer circular boundary $\partial\Omega_2$. The submatrices corresponding to the Dirichlet BCs are obviously unit matrices (still circulant).

3.3. Evaluation of approximation at boundary test points

In the current method we have only evaluated the approximation at nodes in the set \mathcal{X} . In view of the fact that in most BVPs describing physical phenomena the exact solution is not known, to assess the accuracy of the method it is often useful to evaluate the approximation at extra boundary points different than the boundary collocation points (where the exact BC is imposed). This can be achieved easily by simply adding such (extra) boundary collocation points to the set of interior points. In the current context, in order to maintain the block circulant structure of the global matrix, the extra boundary points $\{(x_{mj}, y_{mj})\}_{m=1, j=1}^{M, 2}$ are given by

$$\begin{aligned} x_{mj} &= r_{n_j} \cos\left(\vartheta_m + \frac{2\pi t}{M}\right), & y_{mj} &= r_{n_j} \sin\left(\vartheta_m + \frac{2\pi t}{M}\right), \\ m &= 1, \dots, M, & j &= 1, 2, & n_1 &= 1, & n_2 &= N. \end{aligned} \quad (3.24)$$

Now the parameter t is chosen to be different than s_1 and s_N in (3.3) to avoid coincidence with the current boundary collocation points.

The \mathcal{K}_{int} interior points $\mathcal{X}_{\text{int}} = \{\mathbf{x}_i\}_{i=1}^{\mathcal{K}_{\text{int}}}$ are now taken as the ones defined in (3.4) to which we add the extra boundary points

$$\mathbf{x}_{(N-2)M+(j-1)M+m} = (x_{mj}, y_{mj}), \quad m = 1, \dots, M, \quad j = 1, 2. \quad (3.25)$$

Clearly, now $\mathcal{K}_{\text{int}} = MN$ instead of $M(N-2)$. The nodes on the boundary are constructed as in (3.5) and the total point number is now $M(N+2)$. The details of the implementation are identical to those described in Section 3.2 where the extra boundary points (3.25) are treated as interior points. The resulting global matrix has the same block circulant structure as matrix A in (3.23) but with N replaced with $N+2$. The MDA described in the Appendix can be readily applied to system (3.23) with N replaced with $N+2$.

4. Biharmonic problems – first formulation

4.1. Collocation point distribution

The nodes are constructed as in Section 3.1, see (3.1)-(3.3). The interior nodes $\mathcal{X}_{\text{int}} = \{\mathbf{x}_i\}_{i=1}^{\mathcal{K}_{\text{int}}}$ are, however, now defined from (note that now $\mathcal{K}_{\text{int}} = M(N-4)$)

$$\mathbf{x}_{(n-3)M+m} = (x_{mn}, y_{mn}), \quad m = 1, \dots, M, \quad n = 3, \dots, N-2, \quad (4.1)$$

whilst the boundary nodes $\mathcal{X}_{\text{bry}}^1 = \{\mathbf{x}_i\}_{i=\mathcal{K}_{\text{int}}+1}^{\mathcal{K}_{\text{int}}+\mathcal{K}_{\text{bry}}^1}$ are

$$\mathbf{x}_{(N-4)M+m} = (x_{m1}, y_{m1}), \quad \mathbf{x}_{(N-3)M+m} = (x_{mN}, y_{mN}), \quad m = 1, \dots, M. \quad (4.2)$$

In this case, we also define a second set of boundary points $\mathcal{X}_{\text{bry}}^2 = \{\mathbf{x}_i\}_{i=\mathcal{K}_{\text{int}}+\mathcal{K}_{\text{bry}}^1+1}^{\mathcal{K}_{\text{int}}+\mathcal{K}_{\text{bry}}^1+\mathcal{K}_{\text{bry}}^2}$

$$\mathbf{x}_{(N-2)M+m} = (x_{m1}, y_{m1}), \quad \mathbf{x}_{(N-1)M+m} = (x_{mN}, y_{mN}), \quad m = 1, \dots, M, \quad (4.3)$$

where the points (x_{mi}, y_{mi}) , $m = 1, \dots, M$, $i = 1, 2$ are defined as in (3.24). Fewer interior nodes are considered than in the Laplacian case and a second set of boundary points is included because, in the biharmonic case, two BCs are imposed instead of one. A representative collection of interior and boundary nodes is depicted in Fig. 3(a). Thus, now $\mathcal{X} = \mathcal{X}_{\text{int}} \cup \mathcal{X}_{\text{bry}}^1 \cup \mathcal{X}_{\text{bry}}^2$, $\mathcal{K}_{\text{int}} = (N-4)M$, $\mathcal{K}_{\text{bry}} = \mathcal{K}_{\text{bry}}^1 + \mathcal{K}_{\text{bry}}^2 = 4M$ and $\mathcal{K} = NM$.

4.2. The LMFS

As in Section 3.2 for each node $\mathbf{x}_i \in \mathcal{X}$ we select the κ nearest nodes $\mathcal{X}_i = \{\mathbf{x}_\ell^i\}_{\ell=1}^\kappa$ occupying an area which we shall again denote by Ω_i . Assuming that κ is even, we now choose $\kappa/2$ sources on a circle surrounding Ω_i which we shall denote by $\{\boldsymbol{\xi}_\ell^i\}_{\ell=1}^{\kappa/2}$. These are defined as in (3.6) with κ replaced by $\kappa/2$. Note that, as in the Laplacian case, the number of sources could be taken to be $\kappa_1 < \kappa/2$ without affecting the proposed algorithm. A typical distribution of nodes in Ω_i and the corresponding sources is depicted in Fig. 2(b).

For an interior node $\mathbf{x}_i \in \mathcal{X}_{\text{int}}$, since the solution u satisfies the biharmonic equation, we consider the local MFS approximation

$$u^{(i)}(\mathbf{x}) = \sum_{\ell=1}^{\kappa/2} \alpha_\ell^i G_L(\mathbf{x}, \boldsymbol{\xi}_\ell^i) + \sum_{\ell=1}^{\kappa/2} \beta_\ell^i G_B(\mathbf{x}, \boldsymbol{\xi}_\ell^i), \quad \mathbf{x} \in \bar{\Omega}_i, \quad (4.4)$$

where G_L is a fundamental solution of the Laplace operator defined in (3.8) and G_B is a fundamental solution of the biharmonic operator

$$G_B(\mathbf{x}, \boldsymbol{\xi}) = \frac{1}{8\pi} |\mathbf{x} - \boldsymbol{\xi}|^2 \ln |\mathbf{x} - \boldsymbol{\xi}|, \quad (4.5)$$

while $\{\alpha_\ell^i\}_{\ell=1}^{\kappa/2}$, $\{\beta_\ell^i\}_{\ell=1}^{\kappa/2}$ are unknown coefficients.

We next collocate (4.4) at each of the points \mathbf{x}_ℓ^i , $\ell = 1, \dots, \kappa$, which yields

$$\begin{bmatrix} u^{(i)}(\mathbf{x}_1^i) \\ u^{(i)}(\mathbf{x}_2^i) \\ \vdots \\ u^{(i)}(\mathbf{x}_\kappa^i) \end{bmatrix} = \begin{bmatrix} u_1^{(i)} \\ u_2^{(i)} \\ \vdots \\ u_\kappa^{(i)} \end{bmatrix} = \mathbf{u}^{(i)} = \mathbf{G}_{\text{LB}}^{(i)} \boldsymbol{\gamma}^i, \quad (4.6)$$

where

$$\mathbf{G}_{\text{LB}}^{(i)} = [A_1 \quad A_2],$$

and

$$A_1 = \begin{bmatrix} G_{\text{L}}(\mathbf{x}_1^i - \boldsymbol{\xi}_1^i) & G_{\text{L}}(\mathbf{x}_1^i - \boldsymbol{\xi}_2^i) & \cdots & G_{\text{L}}(\mathbf{x}_1^i - \boldsymbol{\xi}_{\kappa/2}^i) \\ G_{\text{L}}(\mathbf{x}_2^i - \boldsymbol{\xi}_1^i) & G_{\text{L}}(\mathbf{x}_2^i - \boldsymbol{\xi}_2^i) & \cdots & G_{\text{L}}(\mathbf{x}_2^i - \boldsymbol{\xi}_{\kappa/2}^i) \\ \vdots & \vdots & \vdots & \vdots \\ G_{\text{L}}(\mathbf{x}_{\kappa}^i - \boldsymbol{\xi}_1^i) & G_{\text{L}}(\mathbf{x}_{\kappa}^i - \boldsymbol{\xi}_2^i) & \cdots & G_{\text{L}}(\mathbf{x}_{\kappa}^i - \boldsymbol{\xi}_{\kappa/2}^i) \end{bmatrix},$$

$$A_2 = \begin{bmatrix} G_{\text{B}}(\mathbf{x}_1^i - \boldsymbol{\xi}_1^i) & G_{\text{B}}(\mathbf{x}_1^i - \boldsymbol{\xi}_2^i) & \cdots & G_{\text{B}}(\mathbf{x}_1^i - \boldsymbol{\xi}_{\kappa/2}^i) \\ G_{\text{B}}(\mathbf{x}_2^i - \boldsymbol{\xi}_1^i) & G_{\text{B}}(\mathbf{x}_2^i - \boldsymbol{\xi}_2^i) & \cdots & G_{\text{B}}(\mathbf{x}_2^i - \boldsymbol{\xi}_{\kappa/2}^i) \\ \vdots & \vdots & \vdots & \vdots \\ G_{\text{B}}(\mathbf{x}_{\kappa}^i - \boldsymbol{\xi}_1^i) & G_{\text{B}}(\mathbf{x}_{\kappa}^i - \boldsymbol{\xi}_2^i) & \cdots & G_{\text{B}}(\mathbf{x}_{\kappa}^i - \boldsymbol{\xi}_{\kappa/2}^i) \end{bmatrix},$$

$$\boldsymbol{\gamma}^i = \begin{bmatrix} \boldsymbol{\alpha}^i \\ \boldsymbol{\beta}^i \end{bmatrix}, \quad \boldsymbol{\alpha}^i = \begin{bmatrix} \alpha_1^i \\ \alpha_2^i \\ \vdots \\ \alpha_{\kappa/2}^i \end{bmatrix}, \quad \boldsymbol{\beta}^i = \begin{bmatrix} \beta_1^i \\ \beta_2^i \\ \vdots \\ \beta_{\kappa/2}^i \end{bmatrix}.$$

Assuming the $\kappa \times \kappa$ matrix $\mathbf{G}_{\text{LB}}^{(i)}$ is invertible, we have

$$\boldsymbol{\gamma}^i = \mathbf{G}_{\text{LB}}^{(i)-1} \mathbf{u}^{(i)}. \quad (4.7)$$

We now apply (4.4) at the interior point $\mathbf{x} = \mathbf{x}_i$, and from (4.7),

$$\begin{aligned} u^{(i)}(\mathbf{x}_i) &= \sum_{\ell=1}^{\kappa/2} \alpha_{\ell}^i G_{\text{L}}(\mathbf{x}_i, \boldsymbol{\xi}_{\ell}^i) + \sum_{\ell=1}^{\kappa/2} \beta_{\ell}^i G_{\text{B}}(\mathbf{x}_i, \boldsymbol{\xi}_{\ell}^i) \\ &= B_1 \cdot \boldsymbol{\alpha}^i + B_2 \cdot \boldsymbol{\beta}^i \\ &= [B_1 \quad B_2] \boldsymbol{\gamma}^i \\ &= [B_1 \quad B_2] \mathbf{G}_{\text{LB}}^{(i)-1} \mathbf{u}^{(i)} \\ &= \mathbf{v}^{(i)} \mathbf{u}^{(i)} \\ &= \sum_{\ell=1}^{\kappa} v_{\ell}^{(i)} u_{\ell}^{(i)} \end{aligned} \quad (4.8)$$

with

$$B_1 = [G_{\text{L}}(\mathbf{x}_i, \boldsymbol{\xi}_1^i) \quad G_{\text{L}}(\mathbf{x}_i, \boldsymbol{\xi}_2^i) \quad \cdots \quad G_{\text{L}}(\mathbf{x}_i, \boldsymbol{\xi}_{\kappa/2}^i)],$$

$$B_2 = [G_{\text{B}}(\mathbf{x}_i, \boldsymbol{\xi}_1^i) \quad G_{\text{B}}(\mathbf{x}_i, \boldsymbol{\xi}_2^i) \quad \cdots \quad G_{\text{B}}(\mathbf{x}_i, \boldsymbol{\xi}_{\kappa/2}^i)],$$

where the row vector $\mathbf{v}^{(i)}$ is defined by

$$\mathbf{v}^{(i)} := [B_1 \ B_2] \mathbf{G}_{\text{LB}}^{(i)-1}.$$

From (4.8) we obtain a finite difference-type equation linking the approximate values of all nodes in $\Omega^{(i)}$ (including \mathbf{x}_i), and application to every interior node yields the set of equations

$$u^{(i)}(\mathbf{x}_i) - \sum_{\ell=1}^{\kappa} v_{\ell}^{(i)} u_{\ell}^{(i)} = u_i^{(i)} - \sum_{\ell=1}^{\kappa} v_{\ell}^{(i)} u_{\ell}^{(i)} = 0, \quad i = 1, \dots, \mathcal{K}_{\text{int}}. \quad (4.9)$$

To these \mathcal{K}_{int} equations, we add the Dirichlet BCs for $\mathbf{x}_i \in \mathcal{X}_{\text{bry}}^2$

$$u(\mathbf{x}_i) = u_i = g_1^{\text{D}}(\mathbf{x}_i), \quad i = \mathcal{K}_{\text{int}} + \mathcal{K}_{\text{bry}} + 1, \dots, \mathcal{K}_{\text{int}} + \mathcal{K}_{\text{bry}} + \mathcal{K}_{\text{bry}_1}, \quad (4.10)$$

$$u(\mathbf{x}_i) = u_i = g_2^{\text{D}}(\mathbf{x}_i), \quad i = \mathcal{K}_{\text{int}} + \mathcal{K}_{\text{bry}} + \mathcal{K}_{\text{bry}_1} + 1, \dots, \mathcal{K}_{\text{int}} + 2\mathcal{K}_{\text{bry}}. \quad (4.11)$$

Note that the Dirichlet BCs are collocated at the second set of boundary points $\mathcal{X}_{\text{bry}}^2$.

For the Neumann BCs (first biharmonic problem (2.3a)-(2.3b)) we differentiate (4.4) to obtain

$$\frac{\partial u^{(i)}}{\partial \mathbf{n}}(\mathbf{x}) = \sum_{\ell=1}^{\kappa/2} \alpha_{\ell}^i \frac{\partial G_{\text{L}}}{\partial \mathbf{n}}(\mathbf{x}, \boldsymbol{\xi}_{\ell}^i) + \sum_{\ell=1}^{\kappa/2} \beta_{\ell}^i \frac{\partial G_{\text{B}}}{\partial \mathbf{n}}(\mathbf{x}, \boldsymbol{\xi}_{\ell}^i), \quad (4.12)$$

which, when applied on $\partial\Omega_1$ at $\mathbf{x} = \mathbf{x}_i$, $i = M(N-4) + 1, \dots, M(N-3)$ (or $i = \mathcal{K}_{\text{int}} + 1, \dots, \mathcal{K}_{\text{int}} + \mathcal{K}_{\text{bry}_1}$), in combination with (4.6) gives

$$\begin{aligned} g_1^{\text{N}}(\mathbf{x}_i) &= \frac{\partial u^{(i)}}{\partial \mathbf{n}}(\mathbf{x}_i) \\ &= \sum_{\ell=1}^{\kappa/2} \alpha_{\ell}^i \frac{\partial G_{\text{L}}}{\partial \mathbf{n}}(\mathbf{x}_i, \boldsymbol{\xi}_{\ell}^i) + \sum_{\ell=1}^{\kappa/2} \beta_{\ell}^i \frac{\partial G_{\text{B}}}{\partial \mathbf{n}}(\mathbf{x}_i, \boldsymbol{\xi}_{\ell}^i) \\ &= [C_1 \ C_2] \boldsymbol{\gamma}^i \\ &= [C_1 \ C_2] \mathbf{G}_{\text{LB}}^{(i)-1} \mathbf{u}^{(i)} \\ &= \mathbf{v}_{\text{n}}^{(i)} \mathbf{u}^{(i)} \\ &= \sum_{\ell=1}^{\kappa} v_{\ell_{\text{n}}}^{(i)} u_{\ell}^{(i)} \end{aligned} \quad (4.13)$$

with

$$\begin{aligned} C_1 &= \left[\frac{\partial G_{\text{L}}}{\partial \mathbf{n}}(\mathbf{x}_i, \boldsymbol{\xi}_1^i) \ \frac{\partial G_{\text{L}}}{\partial \mathbf{n}}(\mathbf{x}_i, \boldsymbol{\xi}_2^i) \ \dots \ \frac{\partial G_{\text{L}}}{\partial \mathbf{n}}(\mathbf{x}_i, \boldsymbol{\xi}_{\kappa/2}^i) \right], \\ C_2 &= \left[\frac{\partial G_{\text{B}}}{\partial \mathbf{n}}(\mathbf{x}_i, \boldsymbol{\xi}_1^i) \ \frac{\partial G_{\text{B}}}{\partial \mathbf{n}}(\mathbf{x}_i, \boldsymbol{\xi}_2^i) \ \dots \ \frac{\partial G_{\text{B}}}{\partial \mathbf{n}}(\mathbf{x}_i, \boldsymbol{\xi}_{\kappa/2}^i) \right], \end{aligned}$$

where the row vector $\mathbf{v}_n^{(i)}$ is defined by

$$\mathbf{v}_n^{(i)} = [C_1 \ C_2] \mathbf{G}_{\text{LB}}^{(i)-1}$$

and $\partial G_L / \partial n$ is given by (3.19)-(3.20) while

$$\frac{\partial G_B}{\partial n}(\mathbf{x}_i, \boldsymbol{\xi}_\ell^i) = n_{x_i} \frac{\partial G_L}{\partial x}(\mathbf{x}_i, \boldsymbol{\xi}_\ell^i) + n_{y_i} \frac{\partial G_L}{\partial y}(\mathbf{x}_i, \boldsymbol{\xi}_\ell^i)$$

with

$$\begin{aligned} \frac{\partial G_B}{\partial x}(\mathbf{x}, \boldsymbol{\xi}) &= \frac{1}{8\pi} (x - \xi_x) (1 + 2 \ln |\mathbf{x} - \boldsymbol{\xi}|), \\ \frac{\partial G_B}{\partial y}(\mathbf{x}, \boldsymbol{\xi}) &= \frac{1}{8\pi} (y - \xi_y) (1 + 2 \ln |\mathbf{x} - \boldsymbol{\xi}|). \end{aligned} \quad (4.14)$$

From (4.13) we again obtain a finite difference-type equation linking the approximate values of all nodes in $\Omega^{(i)}$ (now excluding the boundary node \mathbf{x}_i), and by applying this to every boundary node on $\partial\Omega_1$, we get the equations

$$\sum_{\ell=1}^{\kappa} v_{\ell_n}^{(i)} u_\ell^{(i)} = g_1^N(\mathbf{x}_i), \quad i = \mathcal{K}_{\text{int}} + 1, \dots, \mathcal{K}_{\text{int}} + \mathcal{K}_{\text{bry}_1}. \quad (4.15)$$

In exactly the same way, by applying (4.12) on $\partial\Omega_2$ at the boundary points $\mathbf{x} = \mathbf{x}_i$, $i = M(N-3) + 1, \dots, M(N-2)$ (or $i = \mathcal{K}_{\text{int}} + \mathcal{K}_{\text{bry}_1} + 1, \dots, \mathcal{K}_{\text{int}} + \mathcal{K}_{\text{bry}}$), we also obtain the set of equations

$$\sum_{\ell=1}^{\kappa} v_{\ell_n}^{(i)} u_\ell^{(i)} = g_2^N(\mathbf{x}_i), \quad i = \mathcal{K}_{\text{int}} + \mathcal{K}_{\text{bry}_1} + 1, \dots, \mathcal{K}_{\text{int}} + \mathcal{K}_{\text{bry}}. \quad (4.16)$$

For the Laplacian operator BCs (second biharmonic problem, (2.3a) and (2.3c)) we differentiate (4.4) to obtain

$$\begin{aligned} \Delta u^{(i)}(\mathbf{x}) &= \sum_{\ell=1}^{\kappa/2} \alpha_\ell^i \Delta G_L(\mathbf{x}, \boldsymbol{\xi}_\ell^i) + \sum_{\ell=1}^{\kappa/2} \beta_\ell^i \Delta G_B(\mathbf{x}, \boldsymbol{\xi}_\ell^i) \\ &= \sum_{\ell=1}^{\kappa/2} \beta_\ell^i \Delta G_B(\mathbf{x}, \boldsymbol{\xi}_\ell^i) \quad (\text{since } \Delta G_L = 0), \end{aligned} \quad (4.17)$$

which, when applied on $\partial\Omega_1$ at $\mathbf{x} = \mathbf{x}_i$, $i = M(N-4) + 1, \dots, M(N-3)$ (or $i = \mathcal{K}_{\text{int}} + 1, \dots, \mathcal{K}_{\text{int}} + \mathcal{K}_{\text{bry}_1}$), in combination with (4.6) gives

$$\begin{aligned} g_1^L(\mathbf{x}_i) &= \Delta u^{(i)}(\mathbf{x}_i) = \sum_{\ell=1}^{\kappa/2} \beta_\ell^i \Delta G_B(\mathbf{x}_i, \boldsymbol{\xi}_\ell^i) \\ &= \left[0 \ 0 \ \cdots \ 0 \mid \Delta G_B(\mathbf{x}_i, \boldsymbol{\xi}_1^i) \ \Delta G_B(\mathbf{x}_i, \boldsymbol{\xi}_2^i) \ \cdots \ \Delta G_B(\mathbf{x}_i, \boldsymbol{\xi}_{\kappa/2}^i) \right] \boldsymbol{\gamma}^i \end{aligned}$$

$$\begin{aligned}
&= \left[0 \ 0 \ \cdots \ 0 \mid \Delta G_B(\mathbf{x}_i, \boldsymbol{\xi}_1^i) \ \Delta G_B(\mathbf{x}_i, \boldsymbol{\xi}_2^i) \ \cdots \ \Delta G_B(\mathbf{x}_i, \boldsymbol{\xi}_{\kappa/2}^i) \right] \mathbf{G}_{LB}^{(i)-1} \mathbf{u}^{(i)} \\
&= \mathbf{v}_L^{(i)} \mathbf{u}^{(i)} \\
&= \sum_{\ell=1}^{\kappa} v_{\ell L}^{(i)} u_{\ell}^{(i)}, \tag{4.18}
\end{aligned}$$

where the row vector $\mathbf{v}_L^{(i)}$ is now defined by

$$\mathbf{v}_L^{(i)} = \left[0 \ 0 \ \cdots \ 0 \mid \Delta G_B(\mathbf{x}_i, \boldsymbol{\xi}_1^i) \ \Delta G_B(\mathbf{x}_i, \boldsymbol{\xi}_2^i) \ \cdots \ \Delta G_B(\mathbf{x}_i, \boldsymbol{\xi}_{\kappa/2}^i) \right] \mathbf{G}_{LB}^{(i)-1}$$

and

$$\Delta G_B(\mathbf{x}, \boldsymbol{\xi}) = \frac{1}{2\pi} (1 + \ln |\mathbf{x} - \boldsymbol{\xi}|). \tag{4.19}$$

From (4.18) we again obtain a finite difference-type equation linking the approximate values of all nodes in $\Omega^{(i)}$ (now excluding the boundary node \mathbf{x}_i), and by applying this to every boundary node on $\partial\Omega_1$, we generate the set of equations

$$\sum_{\ell=1}^{\kappa} v_{\ell L}^{(i)} u_{\ell}^{(i)} = g_1^L(\mathbf{x}_i), \quad i = \mathcal{K}_{\text{int}} + 1, \dots, \mathcal{K}_{\text{int}} + \mathcal{K}_{\text{bry}_1}. \tag{4.20}$$

In exactly the same way, by applying (4.17) on $\partial\Omega_2$ at $\mathbf{x} = \mathbf{x}_i$, $i = M(N-3) + 1, \dots, M(N-2)$ (or $i = \mathcal{K}_{\text{int}} + \mathcal{K}_{\text{bry}_1} + 1, \dots, \mathcal{K}_{\text{int}} + \mathcal{K}_{\text{bry}}$), we also get the set of equations

$$\sum_{\ell=1}^{\kappa} v_{\ell L}^{(i)} u_{\ell}^{(i)} = g_2^L(\mathbf{x}_i), \quad i = \mathcal{K}_{\text{int}} + \mathcal{K}_{\text{bry}_1} + 1, \dots, \mathcal{K}_{\text{int}} + \mathcal{K}_{\text{bry}}. \tag{4.21}$$

We assemble the equations for the \mathcal{K} nodes $\mathbf{x}_i \in \mathcal{X}$, namely (4.9), (4.10)-(4.11), (4.15)-(4.16) or (4.20)-(4.21), and obtain a $\mathcal{K} \times \mathcal{K}$ system of the form (3.22) where $A \in \mathbb{R}^{\mathcal{K} \times \mathcal{K}}$ is sparse and the vector $\mathbf{b} = [b_1, \dots, b_{\mathcal{K}}]^T$ is

$$\begin{aligned}
b_i &= 0, & i &= 1, \dots, \mathcal{K}_{\text{int}}, \\
b_i &= g_1^N(\mathbf{x}_i) \text{ or } g_1^L(\mathbf{x}_i), & i &= \mathcal{K}_{\text{int}} + 1, \dots, \mathcal{K}_{\text{int}} + \mathcal{K}_{\text{bry}_1}, \\
b_i &= g_2^N(\mathbf{x}_i) \text{ or } g_2^L(\mathbf{x}_i), & i &= \mathcal{K}_{\text{int}} + \mathcal{K}_{\text{bry}_1} + 1, \dots, \mathcal{K}_{\text{int}} + \mathcal{K}_{\text{bry}_1} + \mathcal{K}_{\text{bry}_2}, \\
b_i &= g_1^D(\mathbf{x}_i), & i &= \mathcal{K}_{\text{int}} + \mathcal{K}_{\text{bry}} + 1, \dots, \mathcal{K}_{\text{int}} + \mathcal{K}_{\text{bry}} + \mathcal{K}_{\text{bry}_1}, \\
b_i &= g_2^D(\mathbf{x}_i), & i &= \mathcal{K}_{\text{int}} + \mathcal{K}_{\text{bry}} + \mathcal{K}_{\text{bry}_1} + 1, \dots, \mathcal{K}_{\text{int}} + \mathcal{K}_{\text{bry}} + \mathcal{K}_{\text{bry}_1} + \mathcal{K}_{\text{bry}_2}.
\end{aligned}$$

Solving (3.22) for $\mathbf{u}_{\mathcal{K}} \in \mathbb{R}^{\mathcal{K} \times 1}$ determines the approximations at the nodes in set \mathcal{X} . As in the Laplacian case, if $\mathbf{u}_{\mathcal{K}} = [u_{\mathcal{K}_1}, \dots, u_{\mathcal{K}_{\mathcal{K}}}]^T$, then $u_{\mathcal{K}_i}$ is the solution approximation at node \mathbf{x}_i , $i = 1, \dots, \mathcal{K}$.

With the collocation point construction outlined in Section 3.1, the system matrix in (3.22) for the biharmonic BVP possesses the special structure of the system matrix in

(3.23) where the $M \times M$ submatrices A_{n_1, n_2} , $n_1, n_2 = 1, \dots, N$, are, again, sparse and circulant. The block circulant structure of A may be deduced employing arguments similar to those used at the end of Section 3.2 for showing that the corresponding submatrices for the Laplacian are circulant. Consequently, the MDA described in the Appendix may also be employed to solve system (3.23) for the biharmonic BVP efficiently.

5. Biharmonic problems – second formulation

We next propose a second approach for biharmonic BVPs involving a different node configuration. An MDA is still applicable to this approach demonstrating the resilience of the method.

5.1. Collocation point distribution

The interior collocation nodes $\mathcal{X}_{\text{int}} = \{\mathbf{x}_i\}_{i=1}^{\mathcal{K}_{\text{int}}}$ and boundary nodes $\mathcal{X}_{\text{bry}} = \{\mathbf{x}_i\}_{i=\mathcal{K}_{\text{int}}+1}^{\mathcal{K}_{\text{int}}+\mathcal{K}_{\text{bry}}}$ are selected as in Section 3.1, with $\mathcal{K}_{\text{int}} = (N-2)M$, $\mathcal{K}_{\text{bry}} = 2M$ and $\mathcal{K} = NM$. We also define the subset $\mathcal{X}'_{\text{int}}$ of \mathcal{X}_{int} consisting of the $\mathcal{K}'_{\text{int}} = (N-4)M$ interior nodes

$$\mathbf{x}_{(n-2)M+m} = (x_{mn}, y_{mn}), \quad m = 1, \dots, M, \quad n = 3, \dots, N-2. \quad (5.1)$$

5.2. The LMFS

For each node $\mathbf{x}_i \in \mathcal{X}'_{\text{int}} \cup \mathcal{X}_{\text{bry}}$ we select the κ nearest nodes $\mathcal{X}_i = \{\mathbf{x}_\ell^i\}_{\ell=1}^{\kappa}$ occupying an area which we shall again denote by Ω_i . The sources $\{\xi_\ell^i\}_{\ell=1}^{\kappa/2}$ are selected in exactly the same way as in Section 4.2.

For an interior node $\mathbf{x}_i \in \mathcal{X}'_{\text{int}}$ we take the local MFS approximation (4.4) in Ω_i . We follow the same steps as in Section 4.2 except that we do not collocate at all interior nodes \mathcal{X}_{int} but only at the $\mathcal{K}'_{\text{int}} = M(N-4)$ nodes $\mathcal{X}'_{\text{int}}$ (cf. (5.1)). This leads to a set of $\mathcal{K}'_{\text{int}}$ equations of the form (4.9). Note that now, unlike the previous biharmonic formulation, the values of the approximations of u at the points

$$\mathbf{x}_{(n-2)M+m} = (x_{mn}, y_{mn}), \quad m = 1, \dots, M, \quad n = 2, N-1 \quad (5.2)$$

are now also involved, see Fig. 3(b).

The application of the Dirichlet and Neumann (or Laplacian) BCs is identical to the one described in Section 4.2 with the exception that both BCs are applied at the same set of boundary points $\{\mathbf{x}_i\}_{i=\mathcal{K}_{\text{int}}+1}^{\mathcal{K}_{\text{int}}+\mathcal{K}_{\text{bry}}}$. This leads to a set of $2\mathcal{K}_{\text{bry}} = 4M$ equations.

We assemble the equations for the \mathcal{K} nodes $\mathbf{x}_i \in \mathcal{X}'_{\text{int}} \cup \mathcal{X}_{\text{bry}}$ and, noting that we have two BCs at each boundary node, and obtain a $\mathcal{K} \times \mathcal{K}$ system of the form (3.22) where $A \in \mathbb{R}^{\mathcal{K} \times \mathcal{K}}$ is sparse and the vector $\mathbf{b} = [b_1, \dots, b_{\mathcal{K}}]^T$ is now defined as follows:

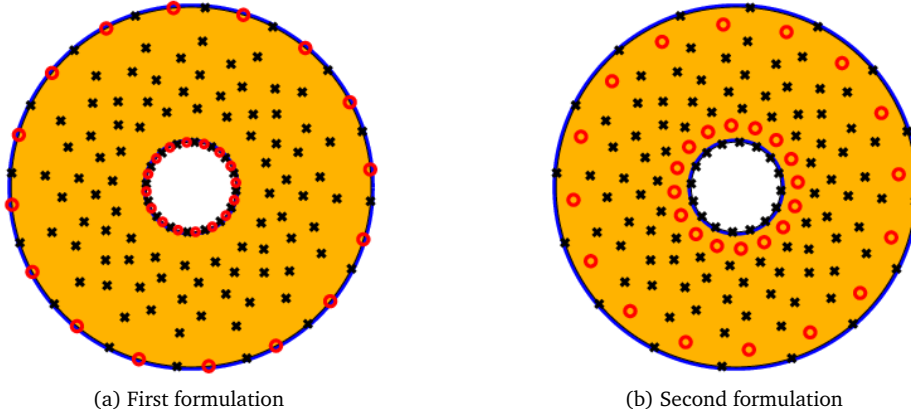


Figure 3: Biharmonic BVPs: (a) Typical collocation point distribution (the second set of boundary points is marked in o) for first formulation and (b) Typical collocation point distribution for second formulation (the interior points where no collocation occurs are denoted by o).

$$\begin{aligned}
 b_i &= 0, & i &= 1, \dots, \mathcal{K}'_{\text{int}}, \\
 b_i &= g_1^{\text{N}}(\mathbf{x}_i) \quad \text{or} \quad g_1^{\text{L}}(\mathbf{x}_i), & i &= \mathcal{K}'_{\text{int}} + 1, \dots, \mathcal{K}'_{\text{int}} + \mathcal{K}_{\text{bry}_1}, \\
 b_i &= g_2^{\text{N}}(\mathbf{x}_i) \quad \text{or} \quad g_2^{\text{L}}(\mathbf{x}_i), & i &= \mathcal{K}'_{\text{int}} + \mathcal{K}_{\text{bry}_1} + 1, \dots, \mathcal{K}'_{\text{int}} + \mathcal{K}_{\text{bry}_1} + \mathcal{K}_{\text{bry}_2}, \\
 b_{\mathcal{K}_{\text{bry}}+i} &= g_1^{\text{D}}(\mathbf{x}_i), & i &= \mathcal{K}'_{\text{int}} + 1, \dots, \mathcal{K}'_{\text{int}} + \mathcal{K}_{\text{bry}_1}, \\
 b_{\mathcal{K}_{\text{bry}}+i} &= g_2^{\text{D}}(\mathbf{x}_i), & i &= \mathcal{K}'_{\text{int}} + \mathcal{K}_{\text{bry}_1} + 1, \dots, \mathcal{K}'_{\text{int}} + \mathcal{K}_{\text{bry}_1} + \mathcal{K}_{\text{bry}_2}.
 \end{aligned}$$

Solving (3.22) for $\mathbf{u}_{\mathcal{K}} \in \mathbb{R}^{\mathcal{K} \times 1}$ yields the approximations at the nodes in \mathcal{X} . Note that now the solution vector \mathbf{u} includes the approximations at all points defined by (3.4) and (3.5), instead of the points in the previous formulation defined by (4.1)-(4.3). As in the previous biharmonic formulation, system (3.23) for the biharmonic BVP can also be solved efficiently using the MDA described in the Appendix.

6. Implementational issues

6.1. Selection of source points

It is well-known that the performance of the MFS is related to the source location and their optimal position has been the subject of intensive research. This is also true of the LMFS where, unlike the traditional MFS where only one set of source points needs to be determined, the source location for each local influence domain needs to be found. In the case of the traditional MFS, in [3], the LOOCV (Leave-One-Out Cross Validation) algorithm was adopted for the determination of a suitable source location. The LOOCV was originally proposed by [32] for the determination of a suitable shape parameter value in RBFs. Clearly, in the case of the local MFS it would be computationally very expensive to determine the optimal source location via LOOCV for each local domain.

As explained in Section 3.2, in each subdomain Ω_i the source points are distributed on a circle centred at the centre point of the sub-domain and with radius R_{mn} , see (3.6). For practical reasons, a unique value R of R_{mn} is often chosen by trial and error or an optimal value of R is chosen, by brute force, by examining the approximation error for a range of values of R . Alternatively, obtaining an appropriate R_{mn} value for the case of the Laplace equation using LOOCV can be performed by the following MATLAB[®] code:

```
% (x,y): points in sub-domain; (x0,y0): centre of sub-domain
% (xs0, ys0): points on unit circle
% pdist2: MATLAB function returning pairwise distance between
    two observation sets
1 function ceps =costEps(ep,x,y,x0,y0,xs0,ys0)
2 xs=x0+xs0*ep; ys=y0+ys0*ep; %source points
3 DM=pdist2([x,y],[xs0,ys0]); %distance matrix
4 A=log(DM);
5 D=pdist2([x0,y0],[xs0,ys0]);
6 rhs=-log(D);
%LOOCV
7 invA=pinv(A);
8 errorvector= (invA*rhs')./diag(invA);
9 ceps=norm(errorvector);
```

where DM in Line 3 is the distance matrix $G_L^{\{i\}}$ and D in Line 5 is the distance vector in (3.13). The cost function costEps is given by

```
R=fminbnd(@(ep) costEps(ep,x,y,x0,y0,xs0,ys0),minR,maxR);
```

where fminbnd is the MATLAB[®] function searching the cost function minimum for the source circle radius R_{mn} and minR and maxR define the initial search interval for R_{mn} . Note that, as already stated, it is impractical to search for a suitable R_{mn} using LOOCV for each sub-main (i.e. $m = 1, \dots, M, n = 1, \dots, N$). To be cost effective, we propose to sampling M sub-domains using LOOCV to determine the corresponding R_{mn} and then taking the average of these radii as the unique R for solving each local matrix system in (3.13). In this work, we chose $M = 10$ and as each local system is small, the additional cost when employing LOOCV is inconsequential. A similar technique may be applied for biharmonic problems.

6.2. Efficient construction of sparse system matrices

In system (3.23), the sparse matrix A has order $MN \times MN$. When M and N are large, despite the sparseness of the matrix A , the memory storage space required is still formidable. However, due to the symmetry of the circularly distributed collocation points, the reduction of the storage required for the matrix A is possible.

More specifically, we observe that on each concentric circle, there are M evenly distributed collocation points. This means that the distribution of the collocation points and corresponding sources in each sub-domain on this circle is identical (see Fig. 7(a) and Remark A.1 in Appendix.) As a result, the M local matrix systems in (3.23) are identical. Hence, we only need to store the local matrix $G_L^{(i)}$ in (3.9) for the Laplacian (and $G_{LB}^{(i)}$ in (4.6) for the biharmonic) once for each concentric circle. Equivalently, we only need to store the first row of each circulant submatrix A_{n_1, n_2} , $n_1, n_2 = 1, \dots, N$, of A in system (3.23). The storage required for the sparse matrix is thus reduced from $MN \times MN$ to $N \times MN$ elements and enormous savings in memory space and CPU running (assembly) time can thus be achieved.

7. Numerical examples

We carried out all numerical experiments with $\varrho_1 = 0.3$ and $\varrho_2 = 1$. Moreover, in the construction of the nodes we took $s_n = (-1)^n/5$, $n = 1, \dots, N$ (cf. (3.3)).

To assess the accuracy of the approximations we computed the maximum relative error E at the nodes comprising \mathcal{X} , defined by

$$E = \frac{\|u - u_\kappa\|_{\infty, \mathcal{X}}}{\|u\|_{\infty, \mathcal{X}}}. \quad (7.1)$$

In this section, all calculations were performed in a notebook computer using MATLAB[®] R2021a with Intel(R) Core(TM) i5-10310 CPU @1.70GHZ, RAM 32 GB, Window 10 Education, 64 bit operation system.

7.1. Example 1

We first study the Dirichlet and the mixed Dirichlet-Neumann BVPs (2.1) for the Laplace equation derived the exact solution

$$u(x, y) = e^x \cos y.$$

We choose the number of nodes in each sub-domain to be $\kappa = 30$ and the same number of source points. As explained in Section 6.1 we place the source points on a circle of radius R centred at the centre of each subdomain (that is we take the same R for each Ω_i). In Fig. 4, we show the accuracy obtained by brute force with respect to varying R for various M and N . We observe that the optimal R is getting smaller when the number of collocation points becomes larger. As the increasing density of the collocation points renders the coefficient matrix in each local system (3.9) more ill-conditioned, the radius of the source circles should be adjusted accordingly.

To properly select the location of the source points for each sub-domain, we also applied LOOCV to determine an appropriate source circle radius R , see Section 6.1. Since we know that as the number of nodes increases the radius is expected to be smaller, we use a smaller upper bound for the search interval for a large number of

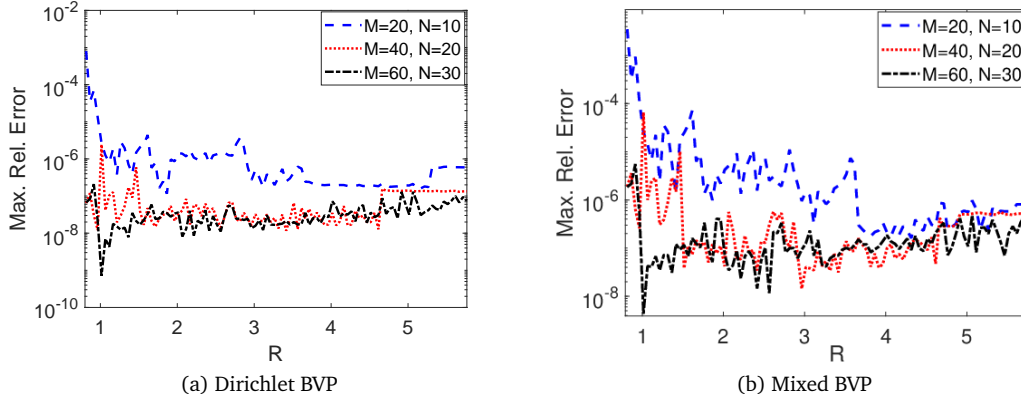


Figure 4: Example 1: Accuracy versus R for various M and N . (a) Dirichlet BVP. (b) Mixed Dirichlet-Neumann BVP.

collocation points. Furthermore, we chose 10 sub-domains, whose centres are equally distributed in $[0.3, 1]$ along the x -axis, and computed the radius for each of these sub-domains using LOOCV and then took the average of these radii as the final radius of each source circle, as described in Section 6.1. In Table 1, we list some results obtained for different M and N for the Dirichlet BVP, using LOOCV and compare these to the results for optimal accuracy obtained (by brute force) in Fig. 4(a). Similar results were obtained for the mixed Dirichlet-Neumann BVP as seen in Table 2.

One of the main advantages of MDAs is that they enable us to handle large-scale problems. To this end, we employ the approach described in Appendix which leads to savings in both computational time and memory storage. For example, for $M = N = 300$, the standard approach forms a sparse matrix of order $300^2 \times 300^2$ containing

Table 1: Example 1: Optimal accuracy results for Dirichlet BVP using LOOCV and brute force.

(M, N)	[min, max]	LOOCV		Optimal	
		R	E	R	E
(20, 10)	[0, 3.0]	2.268	8.863(-7)	1.865	1.152(-7)
(40, 20)	[0, 3.0]	1.925	2.053(-8)	0.965	1.207(-8)
(60, 30)	[0, 1.6]	1.107	3.405(-9)	1.015	7.157(-10)

Table 2: Example 1: Optimal accuracy results for mixed BVP using LOOCV and brute force.

(M, N)	[min, max]	LOOCV		Optimal	
		R	E	R	E
(20, 10)	[0, 4]	3.212	1.807(-7)	4.315	1.609(-7)
(40, 20)	[0, 4]	1.909	5.101(-8)	2.965	4.432(-8)
(60, 30)	[0, 3]	1.363	3.054(-8)	1.015	4.323(-9)

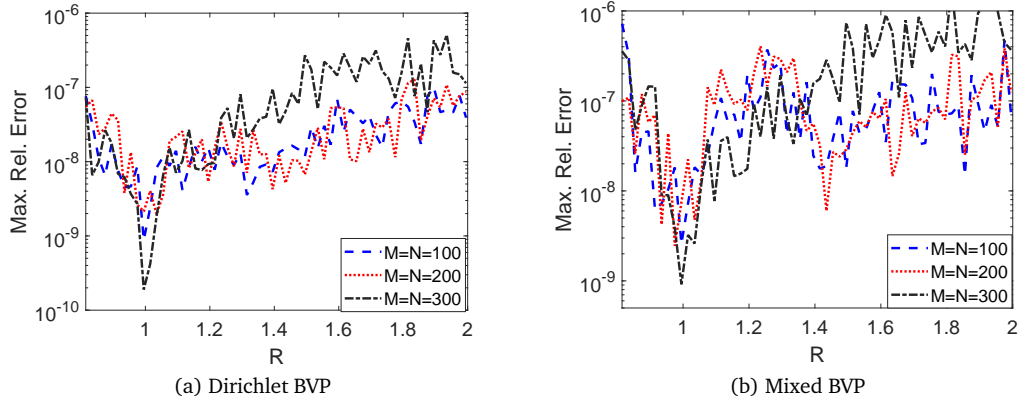


Figure 5: Example 1: Accuracy versus R for various M and N . (a) Dirichlet BVP. (b) Mixed Dirichlet-Neumann BVP.

Table 3: Example 1: Results for Dirichlet and mixed Dirichlet-Neumann BCs using proposed MDA.

$M = N$	[min, max]	Dirichlet BC			Mixed BC		
		R	E	CPU	R	E	CPU
200	[0, 2.0]	0.987	1.693(-9)	0.50	1.210	2.411(-7)	0.54
400	[0, 1.8]	0.937	2.182(-8)	2.99	1.079	7.933(-8)	3.49
600	[0, 1.6]	1.051	6.925(-8)	9.90	0.996	1.571(-8)	9.89
800	[0, 1.6]	1.095	1.207(-8)	23.1	1.074	4.849(-8)	22.9
1000	[0, 1.6]	0.974	8.255(-9)	43.2	0.987	2.474(-8)	42.4

277,2000 nonzero entries while the efficient approach gives a sparse matrix of order $300^2 \times 300^2$ containing only 9240 nonzero entries. In Fig. 5 it is shown that when M and N become large, the optimal R occurs in the neighbourhood of 1. In Fig. 5(a), the optimal values of R for $M = N = 100, 200, 300$ all occur at $R = 0.995$ for the case of Dirichlet BC. Similar results are observed for the mixed BVP where the optimal values of R are 0.995, 0.975, and 0.995, respectively (see Fig. 5(b)). In Table 3, we present results obtained for up to 10^6 nodes, i.e., $M = N = 1000$. We again observe that the LOOCV-predicted R is close to 1 for all cases in this table. One trick which one may employ to reduce the CPU time further is to convert each of the matrices A_m in systems (A.6) in the Appendix to sparse matrices using the MATLAB[®] command `sparse` prior to solving the systems. By doing so, for example, in the case $M = N = 1000$, the CPU time is reduced from 78 to 43 seconds. Furthermore, without the application of the proposed MDA, handling the memory space for a $10^6 \times 10^6$ matrix system would be a challenge even though the global matrix is sparse.

7.2. Example 2

We now examine both BVPs (2.3) for the biharmonic equation derived from the exact solution [11]

$$u(x, y) = \frac{x}{2} (\cos(x) \sinh(y) + \sin(x) \cosh(y)) + 1.$$

In this example, we choose the number of nodes in each sub-domain to be $\kappa = 40$ and the same number of source points. In Fig. 6, we present the accuracy with respect to varying R for three different sets of M and N for the case of the first biharmonic BVP with both the first and second formulations. Unlike the Laplacian case in Example 1, we notice that the optimal R for all three cases occurs at 0.995. Additional tests for various M and N revealed that the optimal R always occurs near 1. In Tables 4 and 5, we demonstrate that the predicted R and accuracy using LOOCV with search interval $[0,2]$ is consistent with the optimal R depicted in Fig. 6.

Next, to show the efficiency of the proposed approaches, we discuss the numerical results issued from large numbers of nodes. In Table 6, we depict the results for the first and second biharmonic BVPs using the first formulation and LOOCV. As was the case for the Laplacian in Example 1, we can handle one million collocation points ($M = N = 1000$) effectively in terms of CPU time and memory space. From this table, we also observe that the obtained optimal values of R using LOOCV are all close to 1 which is consistent with the results shown in Fig. 6. This further confirms that the LOOCV algorithm is a reliable tool for determining an appropriate source location. The accuracy achieved for the first biharmonic BVP is slightly better than that obtained for the second biharmonic BVP.

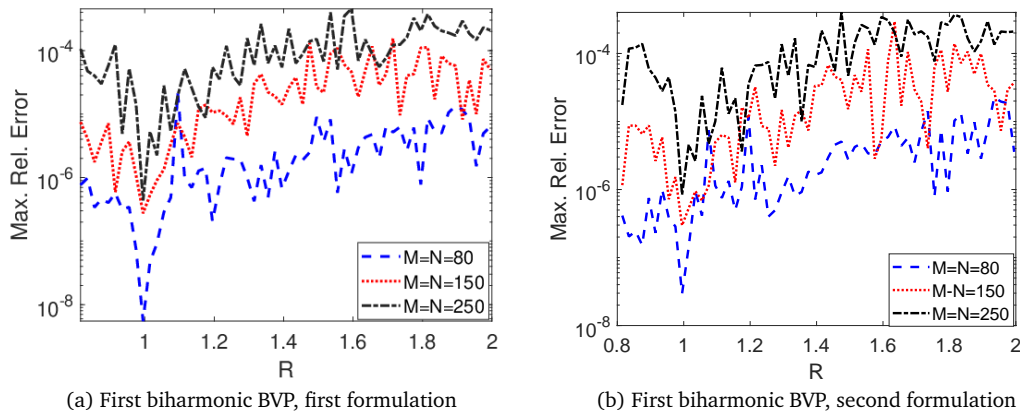


Figure 6: Example 2: Error versus R for first biharmonic BVP.

Table 4: Example 2: Comparison of the optimal accuracy using exhaustive approach and LOOCV for the first biharmonic BVP with first formulation.

$M = N$	Optimal		LOOCV	
	R	E	R	E
80	0.995	5.508(-9)	0.936	3.703(-7)
150	0.995	2.748(-7)	0.966	6.101(-7)
250	0.995	4.359(-7)	0.989	3.064(-6)

The results obtained for the second formulation described in Section 5 are presented in Table 7 and these are similar to those calculated using the first formulation. We again notice that LOOCV yields, as expected, values of R which are located in the neighbourhood of 1.

Table 5: Example 2: Comparison of the optimal accuracy using exhaustive approach and LOOCV for first biharmonic BVP with second formulation.

$M = N$	Optimal		LOOCV	
	R	E	R	E
80	0.995	2.947(-9)	0.998	6.700(-9)
150	0.995	2.966(-7)	0.994	1.378(-7)
250	0.995	8.408(-7)	1.015	3.565(-6)

Table 6: Example 2: Results for first and second biharmonic BVPs using first biharmonic formulation.

$M = N$	[min, max]	First Biharmonic BVP			Second Biharmonic BVP		
		R	E	CPU	R	E	CPU
50	[0, 2.5]	0.982	1.469(-7)	0.12	0.982	4.924(-6)	0.12
100	[0, 2.0]	1.036	1.417(-7)	0.20	1.036	2.967(-7)	0.20
200	[0, 2.0]	1.010	6.099(-7)	0.61	1.010	3.469(-5)	0.57
400	[0, 1.8]	1.036	5.711(-5)	3.18	1.036	1.186(-4)	3.23
600	[0, 1.6]	0.998	4.231(-5)	10.5	0.998	1.566(-4)	9.89
800	[0, 1.6]	0.996	4.735(-4)	24.5	0.996	7.310(-4)	24.4
1000	[0, 1.6]	0.999	4.727(-4)	49.5	0.999	7.387(-4)	49.6

Table 7: Example 2: Results for first and second biharmonic BVPs using second biharmonic formulation.

$M = N$	[min, max]	First Biharmonic BVP			Second Biharmonic BVP		
		R	E	CPU	R	E	CPU
50	[0, 2.5]	1.094	6.084(-6)	0.12	0.995	2.427(-8)	0.12
100	[0, 2.0]	1.026	5.252(-7)	0.20	1.030	1.593(-6)	0.20
200	[0, 2.0]	1.074	2.099(-5)	0.61	0.994	2.028(-7)	0.57
400	[0, 1.8]	1.001	2.458(-5)	3.38	0.937	7.901(-4)	3.69
600	[0, 1.6]	0.994	4.577(-5)	10.5	0.984	1.752(-4)	9.89
800	[0, 1.6]	0.999	4.619(-4)	25.0	0.993	1.620(-4)	26.9
1000	[0, 1.6]	0.965	5.227(-4)	51.5	0.997	4.270(-4)	54.5

8. Conclusions

In this study, the LMFS was applied to Laplacian and biharmonic BVPs in annuli. The collocation points are defined in such a way so that the systems resulting from

the LMFS discretization exhibit special convenient structures. In contrast to the traditional MFS, in the LMFS we adopt the LOOCV to accurately predict the radii of the local source circles. Furthermore, the matrices in these systems are sparse and block circulant and their solution lends itself to the application of MDAs which, as is well-documented, result in considerable savings in both computer time and storage. The combined efficacy of the LMFS and MDA enables us to solve large-scale problems without the need of expensive computer hardware. Clearly, the application of the proposed method to circular disks instead of annular domains is trivial. It is noteworthy that the solution of Laplacian BVPs in more general domains can be obtained via conformal mapping techniques, see [21]. Moreover, the current ideas may be applied readily to the corresponding Helmholtz BVPs as well as higher order polyharmonic and polymeta-harmonic BVPs. Future work will include the application of the proposed method to BVPs in which we have mixed BCs on, say $\partial\Omega_1$, see [20], as well as to 3D axisymmetric BVPs, see e.g. [22].

Appendix

Since matrix A in (3.23) is block circulant, its $M \times M$ circulant submatrices A_{n_1, n_2} can be fully characterized by its first row and will thus be defined by

$$A_{n_1, n_2} = \text{circ} (A_{n_1, n_{21}}, A_{n_1, n_{22}}, \dots, A_{n_1, n_{2M}}), \quad n_1, n_2 = 1, \dots, N. \quad (\text{A.1})$$

In addition, following the description in [27], we denote by U_M the conjugate of the $M \times M$ Fourier matrix [8] and by I_N the identity matrix of order N . Pre-multiplication of system (3.23) by $I_N \otimes U_M$ yields

$$(I_N \otimes U_M) A (I_N \otimes U_M^*) (I_N \otimes U_M) \mathbf{u} = A \mathbf{u} = (I_N \otimes U_M) \mathbf{b} = \mathbf{b}, \quad (\text{A.2})$$

where

$$A = (I_N \otimes U_M) A (I_N \otimes U_M^*) = \begin{bmatrix} D_{1,1} & D_{1,2} & \cdots & D_{1,N} \\ D_{2,1} & D_{2,2} & \cdots & D_{2,N} \\ \vdots & \vdots & & \vdots \\ D_{N,1} & D_{N,2} & \cdots & D_{N,N} \end{bmatrix}, \quad (\text{A.3})$$

where each of the submatrices D_{n_1, n_2} (of order M) is diagonal with

$$D_{n_1, n_2} = \text{diag} (D_{n_1, n_{21}}, D_{n_1, n_{22}}, \dots, D_{n_1, n_{2M}}), \quad n_1, n_2 = 1, \dots, N$$

and from [8]

$$D_{n_1, n_{2m}} = \sum_{k=1}^M A_{n_1, n_{2k}} e^{2\pi(k-1)(m-1)i/M}, \quad m = 1, \dots, M. \quad (\text{A.4})$$

Moreover,

$$\begin{aligned} \mathbf{u} &= \begin{bmatrix} \mathbf{u}_1 \\ \mathbf{u}_2 \\ \vdots \\ \mathbf{u}_N \end{bmatrix} = (I_N \otimes U_M) \mathbf{u} = \begin{bmatrix} U_M \mathbf{u}_1 \\ U_M \mathbf{u}_2 \\ \vdots \\ U_M \mathbf{u}_N \end{bmatrix}, \\ \mathbf{b} &= \begin{bmatrix} \mathbf{b}_1 \\ \mathbf{b}_2 \\ \vdots \\ \mathbf{b}_N \end{bmatrix} = (I_N \otimes U_M) \mathbf{b} = \begin{bmatrix} U_M \mathbf{b}_1 \\ U_M \mathbf{b}_2 \\ \vdots \\ U_M \mathbf{b}_N \end{bmatrix}. \end{aligned} \quad (\text{A.5})$$

The basic steps in the MDA can be described as follows:

Step 1. We calculate $\mathbf{b}_n = U_M \mathbf{b}_n$, $n = 1, \dots, N$ in (A.5). These operations can be performed efficiently using the MATLAB[®] command `fft`. Note that in practice we do not need to calculate \mathbf{b}_n for $n = 1, \dots, N$ as most of the vectors \mathbf{b}_n are zeros vectors. For example, in Laplacian case we only need to calculate $\mathbf{b}_n = U_M \mathbf{b}_n$, $n = 1, 2$, which results in further savings in computational time.

Step 2. We compute the diagonal matrices D_{n_1, n_2} from (A.4). These operations can be carried out efficiently using the MATLAB[®] command `ifft`. The matrix A in (3.23) is sparse and, as a result, several of the row vectors in (A.1) which determine each circulant submatrix A_{n_1, n_2} are zero. Hence, not all elements $D_{n_1, n_2, m}$ in (A.4) need to be calculated. Thus, additional savings can be achieved by introducing an `if` statement in the appropriate position, as shown in line 11 of the MATLAB[®] code listed at the end of this Appendix.

Step 3. Matrix A in (A.2) is made up of N^2 diagonal blocks of order M . Hence, system (A.2) may be broken into M independent $N \times N$ sub-systems, namely,

$$A_m \mathbf{u}_m = \mathbf{b}_m, \quad m = 1, \dots, M, \quad (\text{A.6})$$

where

$$(A_m)_{n_1, n_2} = D_{n_1, n_2, m}, \quad n_1, n_2 = 1, \dots, N,$$

and

$$(\mathbf{u}_m)_n = (\mathbf{u}_n)_m, \quad (\mathbf{b}_m)_n = (\mathbf{b}_n)_m, \quad n = 1, \dots, N. \quad (\text{A.7})$$

Solving systems (A.6) is the costliest part of the MDA as it involves solving M linear $N \times N$ systems. However, each matrix A_m , $m = 1, \dots, M$, is sparse and use of the MATLAB[®] `sparse` command in solving systems (A.6) yields further savings.

Step 4. From (A.7) we obtain the vectors \mathbf{u}_n , $n = 1, \dots, N$ and from these \mathbf{u} from (A.5), with $\mathbf{u}_n = U_M^* \mathbf{u}_n$, $n = 1, \dots, N$. These operations can be carried out efficiently using the MATLAB[®] command `ifft`.

Remark A.1. In addition to the savings in computational time, we also obtained substantial storage savings because only the first row (A.1) of each of the sparse circulant submatrices A_{n_1, n_2} must be constructed and stored. From symmetry, see Fig. 7(a), and as explained in Section 3.2, the node distribution in any two influence domains whose centres lie on the same circle is identical. Clearly, this is also true of the corresponding surrounding sources (under appropriate rotation). It is therefore only necessary to use the N red centre points in Fig. 7(b) along with the collocation points in their influence domains and corresponding surrounding sources for the construction of the first row of each sparse circulant MFS interpolation submatrix.

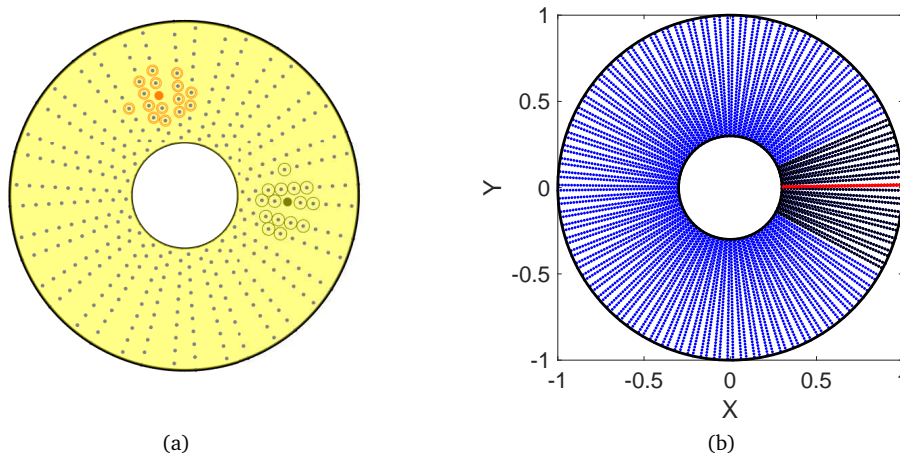


Figure 7: (a) Identical influence domains whose centres lie on the same circle. (b) Only one row of the sparse circulant sub-matrix is required for the formulation of the MFS interpolation matrix.

The implementation of the MDA steps is presented in following MATLAB[®] code:

```
% A: sparse LMFS matrix with order n x nm
% B: Boundary conditions
% nr: number of concentric circles;
% nc: number of collocation points in each concentric circle
1 function solution=MDA(A,B,nr,nc)
2 n=nr; m=nc; b=sparse(n,m);
3 b1=[B(1:m,1) B(m+1:2*m,1)];
4 b(1:2,1:m)=transpose(fft(b1(1:m,1:2))/sqrt(m));
5 b=sparse(b);
6 D=zeros(nr,nr,nc);
7 for in=1:nr
8     temp=(A(in,:))'; temp=reshape(temp,nc,nr);
9     T=sum(temp) ;
10    for jn=1:nr
11        if T(jn) ~=0
```

```

12         D(in,jn,:)=ifft(full(temp(:,jn)))*nc;
13     end
14 end
15 end
16 sol=zeros(m,n);
17 for ii=1:m
18     sol(ii,:)=sparse(D(:,:,ii))\b(:,ii); % solution of subsystems
19 end

```

References

- [1] B. BIALECKI, G. FAIRWEATHER, AND A. KARAGEORGHIS, *Matrix decomposition algorithms for elliptic boundary value problems: A survey*, Numer. Algorithms 56 (2011), 253–295.
- [2] C. S. CHEN AND A. KARAGEORGHIS, *Local RBF algorithms for elliptic boundary value problems in annular domains*, Commun. Comput. Phys. 25 (2019), 41–67.
- [3] C. S. CHEN, A. KARAGEORGHIS, AND Y. LI, *On choosing the location of the sources in the MFS*, Numer. Algorithms 72 (2016), 107–130.
- [4] Z. CHEN AND F. WANG, *On the supporting nodes in the localized method of fundamental solutions for 2D potential problems with Dirichlet boundary condition*, AIMS Math. 6 (2021), 7056–7069.
- [5] Z. CHEN AND F. WANG, *Localized method of fundamental solutions for acoustic analysis inside a car cavity with sound-absorbing material*, Adv. Appl. Math. Mech. 15 (2023), 182–201.
- [6] Z. CHEN, F. WANG, S. CHENG, AND G. WU, *Localized MFS for three-dimensional acoustic inverse problems on complicated domains*, Int. J. Mech. Syst. Dyn. 2 (2022), 143–152.
- [7] A. H. D. CHENG AND Y. HONG, *An overview of the method of fundamental solutions-solvability, uniqueness, convergence and stability*, Eng. Anal. Bound. Elem. 120 (2020), 118–152.
- [8] P. J. DAVIS, *Circulant Matrices*, AMS Chelsea Publishing, 1994.
- [9] G. FAIRWEATHER AND R. L. JOHNSTON, *The method of fundamental solutions for problems in potential theory*, in: Treatment of Integral Equations by Numerical Methods, C. T. H. Baker and G. F. Miller (Eds.), Academic Press (1982), 349–359.
- [10] G. FAIRWEATHER AND A. KARAGEORGHIS, *The method of fundamental solutions for elliptic boundary value problems*, Adv. Comput. Math. 9 (1998), 69–95.
- [11] C. M. FAN, Y. K. HUANG, C. S. CHEN, AND S. R. KUO, *Localized method of fundamental solutions for solving two-dimensional Laplace and biharmonic equations*, Eng. Anal. Bound. Elem. 101 (2019), 188–197.
- [12] Z. FAN, Y. LIU, A. HONG, F. XU, AND F. WANG, *The localized method of fundamental solutions for two dimensional Signorini problems*, CMES-Comput. Model. Eng. Sci. 132 (2022), 341–355.
- [13] J. H. FRIEDMAN, J. BENTLEY, AND R. A. FINKEL, *An algorithm for finding best matches in logarithmic expected time*, ACM Trans. Math. Software 3 (1977), 209–226.
- [14] M. A. GOLBERG AND C. S. CHEN, *The method of fundamental solutions for potential, Helmholtz and diffusion problems*, Boundary Integral Methods: Numerical and Mathematical Aspects, M. A. Golberg (Ed.), Comput. Eng., Vol. 1, WIT Press/Comput. Mech. Publ., Boston, MA (1999), 103–176.

- [15] Y. GU, C. M. FAN, AND Z. FU, *Localized method of fundamental solutions for three-dimensional elasticity problems: Theory*, Adv. Appl. Math. Mech. 13 (2021), 1520–1534.
- [16] Y. GU, C. M. FAN, W. Z. QU, AND F. WANG, *Localized method of fundamental solutions for large-scale modelling of three-dimensional anisotropic heat conduction problems – Theory and MATLAB code*, Comput. Struct. 220 (2019), 144–155.
- [17] Y. GU, C. M. FAN, W. QU, F. WANG, AND C. ZHANG, *Localized method of fundamental solutions for three-dimensional inhomogeneous elliptic problems: Theory and MATLAB code*, Comput. Mech. 64 (2019), 1567–1588.
- [18] Y. GU, C. M. FAN, AND R. P. XU, *Localized method of fundamental solutions for large-scale modeling of two-dimensional elasticity problems*, Appl. Math. Lett. 93 (2019), 8–14.
- [19] Y. GU, M. V. GOLUB, AND C. M. FAN, *Analysis of in-plane crack problems using the localized method of fundamental solutions*, Eng. Fract. Mech. 256 (2021), 107994.
- [20] A. KARAGEORGHIS, *The method of fundamental solutions for elliptic problems in circular domains with mixed boundary conditions*, Numer. Algorithms 68 (2015), 185–211.
- [21] A. KARAGEORGHIS AND Y.-S. SMYRLIS, *Conformal mapping for the efficient MFS solution of Dirichlet boundary value problems*, Computing 83 (2008), 1–24.
- [22] A. KARAGEORGHIS, C. S. CHEN, AND X-Y. LIU, *Kansa-RBF algorithms for elliptic problems in axisymmetric domains*, SIAM J. Sci. Comput. 38 (2016), A435–A470.
- [23] W. LI, *Localized method of fundamental solutions for 2D harmonic elastic wave problems*, Appl. Math. Lett. 112 (2021), 106759.
- [24] X. LI AND S. LI, *On the augmented moving least squares approximation and the localized method of fundamental solutions for anisotropic heat conduction problems*, Eng. Anal. Bound. Elem. 119 (2020), 74–82.
- [25] Q. G. LIU, C. M. FAN, AND B. ŠARLER, *Localized method of fundamental solutions for two-dimensional anisotropic elasticity problems*, Eng. Anal. Bound. Elem. 125 (2021), 59–65.
- [26] S. LIU, P. W. LI, C. M. FAN, AND Y. GU, *Localized method of fundamental solutions for two- and three-dimensional transient convection-diffusion-reaction equations*, Eng. Anal. Bound. Elem. 124 (2021), 237–244.
- [27] X-Y. LIU, A. KARAGEORGHIS, C. S. CHEN, *A Kansa-radial basis function method for elliptic boundary value problems in annular domains*, J. Sci. Comput. 65 (2015), 1240–1269.
- [28] R. MATHON AND R. L. JOHNSTON, *The approximate solution of elliptic boundary-value problems by fundamental solutions*, SIAM J. Numer. Anal. 14 (1977), 638–650.
- [29] W. QU, C. M. FAN, AND Y. GU, *Localized method of fundamental solutions for interior Helmholtz problems with high wave number*, Eng. Anal. Bound. Elem. 107 (2019), 25–32.
- [30] W. QU, C. M. FAN, Y. GU, AND F. WANG, *Analysis of three-dimensional interior acoustic fields by using the localized method of fundamental solutions*, Appl. Math. Model. 76 (2019), 122–132.
- [31] W. QU, C. M. FAN, AND X. LI, *Analysis of an augmented moving least squares approximation and the associated localized method of fundamental solutions*, Comput. Math. Appl. 80 (2020), 13–30.
- [32] S. RIPPA, *An algorithm for selecting a good value for the parameter c in radial basis function interpolation*, Adv. Comput. Math. 11(2-3) (1999), 193–210.
- [33] L. SUN, Z. FU, AND Z. CHEN, *A localized collocation solver based on fundamental solutions for 3D time harmonic elastic wave propagation analysis*, Appl. Math. Comput. 439 (2023), 127600.
- [34] F. WANG, C. M. FAN, Q. HUA, AND Y. GU, *Localized MFS for the inverse Cauchy problems of two-dimensional Laplace and biharmonic equations*, Appl. Math. Comput. 364 (2020), 124658.

- [35] J. ZHANG, C. YANG, H. ZHENG, C. M. FAN, AND M. F. FU, *The localized method of fundamental solutions for 2D and 3D inhomogeneous problems*, Math. Comput. Simul. 200 (2022), 504–524.
- [36] J. ZHANG, H. ZHENG, C. M. FAN, AND M. F. FU, *The localized method of fundamental solutions for two-dimensional inhomogeneous inverse Cauchy problems*, Mathematics 10 (2022), 1464.